Eurasian Chem.-Technol. J. 27 (2025) 159–171
The journal of the Institute of Combustion Problems https://ect-journal.kz

https://doi.org/10.18321/ectj1663

Electrochemical Behaviour of Commercial and Modified Activated Carbons in Aqueous Supercapacitors

K.M. Temirkulova[1,2], S. Temirbolat[2], Zh.A. Supiyeva[1,2]*, Q. Abbas[3,4]

[1]Satbayev University, 22a Satpaev Str., 050013, Almaty, Kazakhstan
[2]Al-Farabi Kazakh National University, 71 Al-Farabi Ave., 050040, Almaty, Kazakhstan
[3]Graz University of Technology, Stremayrgasse 9, 8010 Graz, Austria
[4]Poznan University of Technology, Berdychowo 4, 60-965 Poznań, Poland

Article info

Received:
5 March 2025

Received in revised form:
19 April 2025

Accepted:
6 July 2025

Keywords:
Supercapacitors
Activated carbon
Heat treatment
Porous structure
Cycling resistance

Abstract

Supercapacitors offer high specific power, short charge-discharge times, and long cycle life. This study presents a comparative analysis of the electrochemical performance of commercial activated carbon Kuraray YP80F and its modified analogue YP80FP, which was subjected to thermal treatment. High-temperature treatment of YP80FP led to changes in porosity and a reduction in electrochemical activity. Electrochemical studies were carried out using cyclic voltammetry, galvanostatic charge-discharge, electrochemical impedance spectroscopy, and self-discharge methods. The results show that YP80F exhibits higher specific capacitance and lower internal resistance owing to its well-developed microporous structure. The optimum operating voltage range was determined to be between 0.6–1.5 V, with YP80F showing the best performance for an aqueous sodium nitrate electrolyte. The results demonstrate that heat treatment of activated carbon may lead to the development of surface functional groups and the blocking of pores, affecting overall supercapacitor performance in aqueous electrolytes.

1. Introduction

In recent decades, global energy consumption has increased rapidly. Population growth and technological advances have intensified dependence on fossil fuels, which are not only limited in supply but also cause severe environmental damage. Consequently, scientific research has increasingly focused on the development of sustainable and renewable energy technologies, such as solar, wind, and hydropower systems. However, the large-scale adoption of renewable sources requires the implementation of efficient energy storage systems to ensure grid stability and energy availability. These technologies are regarded as promising solutions for clean energy storage [1–4].

Among the various energy storage approaches, electrochemical devices are of particular interest due to their high energy-conversion efficiency, scalability, and cost-effectiveness [5–6].

Supercapacitors operate primarily through non-Faradaic mechanisms (electrochemical double-layer capacitance), enabling rapid ion adsorption and desorption at the electrode–electrolyte interface. Unlike batteries, supercapacitors offer advantages such as short charging and discharging times, long service life, low weight, and environmental friendliness. However, supercapacitors have a much lower energy density (0.5–30 Wh/kg), although they can rapidly release stored energy over short time periods [7]. Rechargeable batteries are commonly used in electric vehicles, portable electronics, and grid applications. Nevertheless, they suffer from drawbacks such as long charging times, limited lifespan, safety concerns, and thermal management issues [8, 9].

One of the main advantages of supercapacitors is their extremely high cycling resistance – they can withstand up to 500,000 charge-discharge cycles, whereas lithium-ion batteries are limited to 800–3000 cycles [10, 11]. Supercapacitors also superior in power density (13 kW/kg compared to 0.5–1 kW/kg for Li-ion batteries) [12, 13]. Their high

*Corresponding author.
E-mail address: Zhazira.Supiyeva@kaznu.edu.kz

© 2025 The Author(s). Published by al-Farabi Kazakh National University
This is an open access article under the CC BY 4.0 (http://creativecommons.org/licenses/by/4.0/)

power and low internal resistance provide them with fast charging and discharging times ranging from 0.3 to 30 sec, while this process takes 0.3 to 3 h for Li-ion batteries [14]. Regarding capital costs, the price range of both types of devices is quite wide. Li-ion batteries have energy storage costs in the range of 600–2500 $/kW·h, whereas supercapacitors range from 300 to 2000 $/kW·h [15, 16]. In the long run, supercapacitors may be more favorable given their long lifetime and minimal maintenance costs. While Li-ion batteries typically have a life expectancy of 14–16 years, they often exhibit performance degradation over time. In contrast, supercapacitors can operate for nearly 20 years with minimal loss of performance throughout their service life [17, 18].

In this context, porous carbon materials have attracted much attention due to their unique characteristics. Some of their advantages include low cost, high chemical stability, environmental friendliness, excellent electrical and thermal conductivity, high chemical stability, light weight, diversity of structures, advanced porosity and the ability to adjust it using different synthesis methods from a variety of precursors [17-19].

According to IUPAC recommendations, porous carbon materials are classified by pore size into three categories: micropores (<2 nm), mesopores (2–50 nm) and macropores (> 50 nm) [20]. In general, micropores function as active centers, playing a key role in catalysis and providing selectivity in size and shape of molecules. Mesopores promote efficient mass transfer and facilitate access to functional centers, while macropores allow rapid diffusion of molecules such as oxygen in oxygen reduction reactions [21, 22]. Some carbon materials, such as carbon aerogels, have a hierarchical structure with developed porosity and a wide distribution of pore sizes in a single material, which favours accelerated mass transfer and increased available surface area for efficient chemical reactions [23, 24].

Nevertheless, for successful commercialisation of supercapacitors, significant research efforts are needed to address their technical shortcomings. An important characteristic of supercapacitors is the choice of electrolyte. Recently, aqueous electrolytes are again considered as a suitable alternative to organic electrolytes due to their high ionic conductivity, low cost, environmental friendliness, high mobility and lack of toxicity [25, 26]. The use of 5M $NaNO_3$ increases ionic strength and conductivity, reducing internal resistance and enhancing charge/discharge performance. Unlike organic and ionic liquids, which require complex purification procedures, aqueous electrolytes are widely used in both research and industrial applications. Their high electrical conductivity reduces the equivalent series resistance, which improves the power distribution of supercapacitors [27].

In addition, aqueous alkaline ion batteries utilise materials with an operating potential between the O_2 and H_2 release potentials. The choice of electrode materials can be adapted depending on the pH of the medium, which is related to the oxygen and hydrogen evolution potentials in aqueous systems [28]. For example, Jabeen [29] and Xiong [30] investigated the electrochemical properties of asymmetric aqueous supercapacitors, showing the efficiency of a 2.6 V cell with $Na_{0.5}MnO_2$ as cathode and Fe_3O_4 coated with carbon as anode [29]. These include KOH, Na_2SO_4, H_2SO_4, Li_2SO_4, KCl, LiCl, and nitrates such as $NaNO_3$ and $LiNO_3$, among others [31].

The most important performance parameters of supercapacitors from practical point of view include energy density, and other important parameters such as capacitance, equivalent series resistance, power density, operating temperature range, cycling and self-discharge rate [32]. In this regard, the aim of this work is to comparatively analyse the electrochemical performance of commercial activated carbon YP80F and its heat-treated counterpart YP80FP in aqueous supercapacitors, focusing on how heat treatment alters porosity and surface characteristics, and how these changes influence the overall performance of supercapacitor electrodes.

2. Experimental section

2.1 Materials

Commercial activated carbon Kuraray YP80F and its thermally treated analogue YP80FP were used as electrode materials. Thermal treatment was carried out at 800 °C for 1 h in a nitrogen atmosphere to modify the porous structure. The process involved heating at 10 °C/min to 800 °C, holding for 1 h, and cooling at 5 °C/min under a continuous nitrogen flow (150 mL/min). Treatment was performed in a CVD furnace with quartz tube and temperature controller. Gas was supplied through a rotameter ensuring stable flow. YP80F is characterized by a high specific surface area and developed microporosity, which promote effective charge storage.

2.2 Preparation of electrodes

The working electrodes were prepared by mixing the following components: 90 wt.% activated

carbon, 5 wt.% carbon black (Acetylene Black, used as a conductive additive to improve electrical conductivity) and 5 wt.% polytetrafluoroethylene (PTFE, 60 wt.% dispersion in water, Sigma-Aldrich, part number 665800-100ML). The mixture was dispersed in ethanol to form a slurry, followed by ultrasonic treatment for 10 min to provide a homogeneous dispersion. The electrodes were formed by rolling the carbon mixture on steel rollers to a thickness of 150 µm, which provided uniform material distribution and improved mechanical stability. The rolled electrodes were dried in a desiccator at 90 °C for 12 h to remove residual moisture and solvent. After drying, the electrodes were cut with 9 mm diameter steel punches to obtain working discs. Geometry was checked using caliper and micrometer to ensure dimensional accuracy. The electrodes were then weighed on an analytical balance with an accuracy of 0.1 mg for further electrochemical studies.

2.3 Equipment and methods

Nitrogen adsorption-desorption isotherms at 77.3 K were recorded using a Micromeritics ASAP 2020 surface and porosity analyzer (software version V4.01). Prior to analysis, samples were degassed in a vacuum according to standard procedure. The specific surface area was calculated using the BET method, and the pore volume and distribution were calculated using the BJH method during the desorption stage. The surface morphology of carbon materials was studied by scanning electron microscopy (SEM) using a JEOL JSM-6490LA electron microscope at an accelerating voltage of 30 kV. The images were taken in high vacuum mode at a magnification of ×2000. The images obtained were used to evaluate the surface structure and pore distribution. Electrochemical measurements, including cyclic voltammetry (CV), galvanostatic charge-discharge (GCD), and electrochemical impedance spectroscopy (EIS), were performed using a BioLogic VMP3 potentiostat/galvanostat. The measurements were performed in a two-electrode cell in which both electrodes were made of the carbon material under investigation. An aqueous solution was used as the electrolyte, and all tests were performed at room temperature.

3. Results and Discussion

3.1 Textural characteristics by BET analysis

The results of the texture analysis are presented in Table 1 and Fig. 1. The YP80F sample demonstrated a high specific surface area according to BET (2346.1 m^2/g), while the heat-treated analogue YP80FP had a specific surface area of 2414.8 m^2/g. The slight decrease in the total pore volume and micropore volume in YP80FP may be due to the partial loss of volatile components and the compaction of the structure during heat treatment. The pore size distribution according to the BJH model is shown in Fig. 1b and indicates the preservation of the mesoporous structure in both samples with a dominant pore size of about 2.3–2.4 nm.

The nitrogen adsorption-desorption isotherms (Fig. 1a) for both samples correspond to the IUPAC type I/IV isotherm, confirming the presence of both micropores and mesopores. A slight shift in the YP-80FP curve indicates a change in the pore structure under the influence of heat treatment, which is confirmed by an increase in the proportion of pores with a diameter of less than 2 nm.

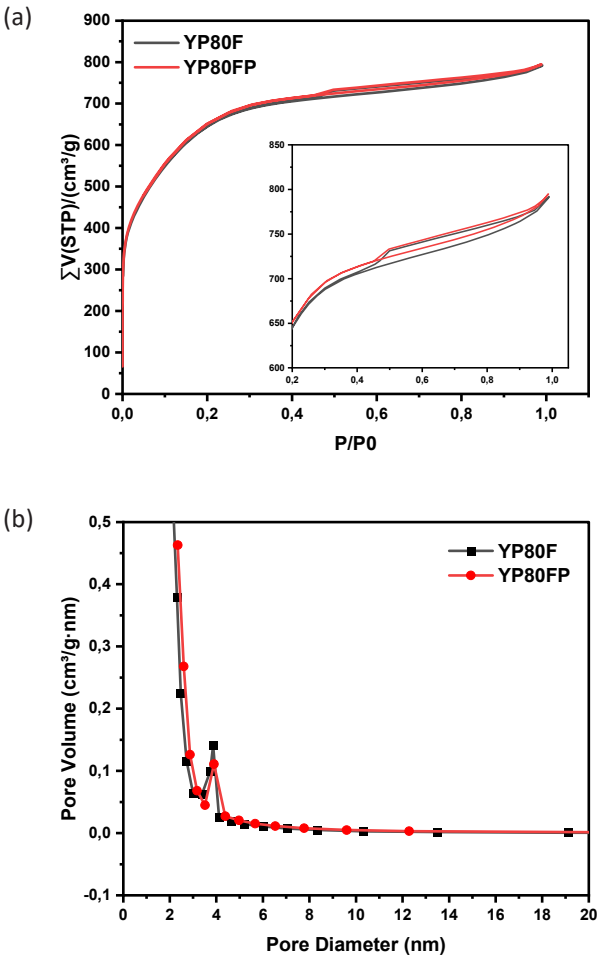

Fig. 1. a) Isotherms of nitrogen adsorption-desorption of YP80F and YP80FP samples; b) Distribution of pore volume depending on pore diameter (BJH method, desorption).

Table 1. Textural parameters of YP80F and YP80FP

Carbon	S_{BET}, m^2/g	Micro volume (V_{micro}), cm^3/g	Meso volume (V_{meso}), cm^3/g	Total volume (V_t), cm^3/g	% (V_{micro}/V_t)	Average pore diameter, nm
YP80F	2346.1	0.9711	0.2531	1.2242	79.3%	2.09
YP80FP	2414.79	1.0012	0.2349	1.2361	81.0%	2.04

The results of BET analysis show that heat treatment does not lead to significant degradation or loss of microporosity but allows the structural parameters to be maintained at a high level. This confirms that YP80F has high thermal stability and the modified YP80FP carbon can be used in the same sorption and electrochemical applications as the original material.

3.2 Analysis of surface morphology

Scanning electron microscopy (SEM) analysis was performed to investigate the structural differences between YP80F commercial activated carbon and its modified analogue YP80FP. Two scales were chosen for each sample: 1000× and 2000×, which allowed the evaluation of changes on both micro- and nanoscales.

In Fig. 2a, the surface of YP80F at 1000× magnification shows irregularly shaped agglomerates of particles forming a loose, porous structure. The surface is inhomogeneous, containing cracks, furrows and depressions indicating developed microporosity. Fig. 2b at 2000×, a fine texture of the carbon surface with many small irregular pores embedded in the framework is visible. This microstructure indicates a high degree of activation and is consistent with the results of BET analysis.

In Fig. 3a at 1000× magnification, the surface of YP80FP appears more dense and smoothed compared to the original material. The particles are more compact and the degree of surface texturing is reduced, indicating thermal densification of the structure. Fig. 3b at 2000× shows a smooth, ordered surface with less pronounced pores. This may be due to partial baking of the pore walls, although the microporous structure is generally preserved, as confirmed by BET data.

SEM images confirmed the YP80F sample has a loose and highly textured surface characteristic of highly activated carbon materials with pronounced microporosity. After heat treatment at 800 °C (YP-80FP), the surface structure became denser and smoother, with less pronounced pore elements. Despite these morphological changes, the internal microporous architecture of the material is preserved, which is consistent with the textural characteristics obtained by BET. Thus, heat treatment affects mainly the external morphology without disturbing the functional structure of the pore space.

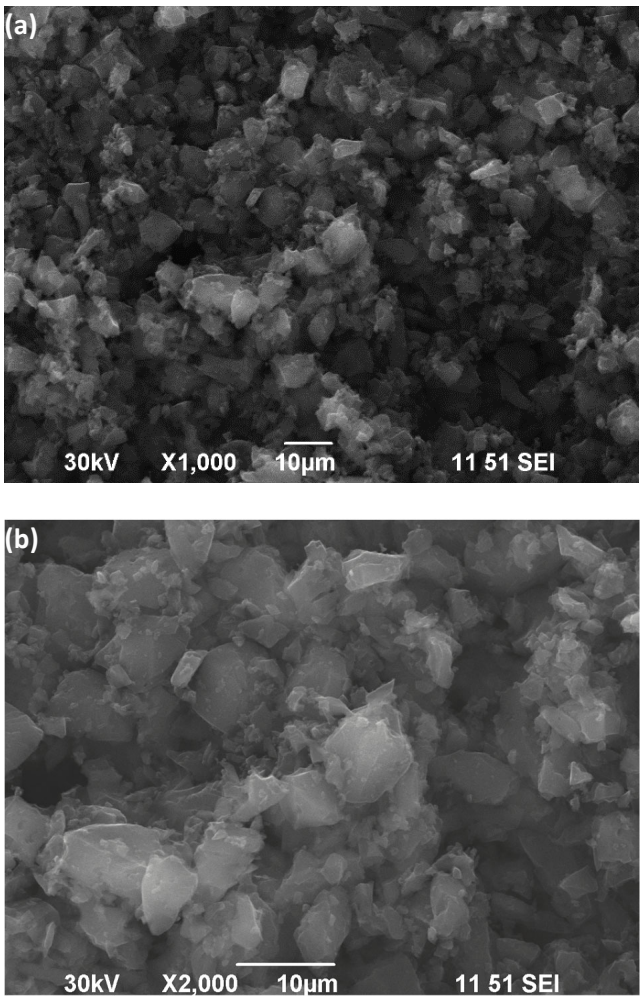

Fig. 2. Surface morphology of Kuraray YP80F carbon starting material at 1000× magnification (a) and at 2000× magnification (b).

3.3 Electrochemical Performance of YP80F and YP80FP

Sodium nitrate ($NaNO_3$) was selected as the aqueous electrolyte due to its neutral pH, high ionic conductivity, chemical stability, and compatibility with both carbon-based electrodes and stainless

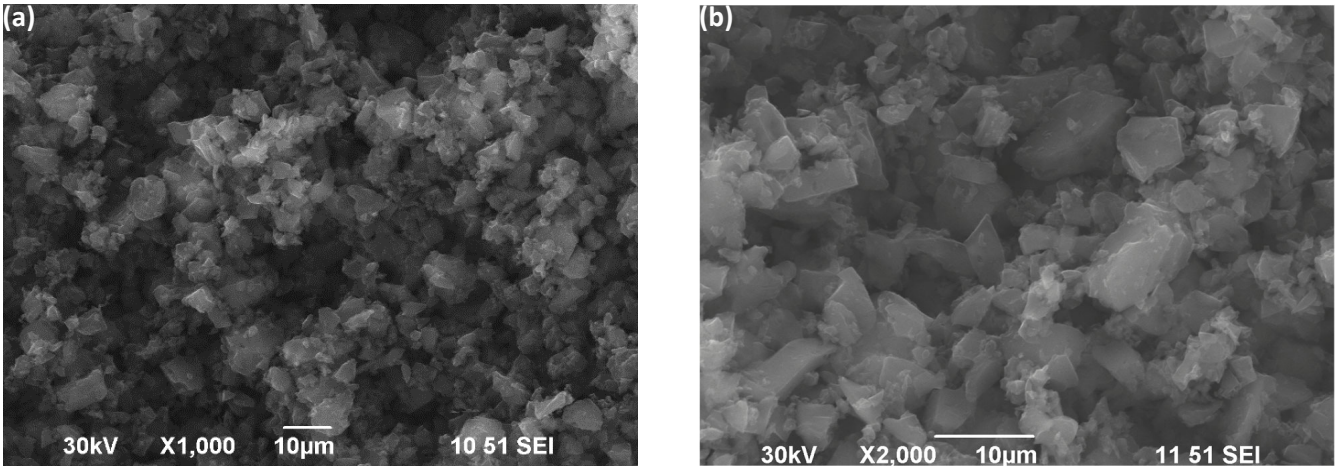

Fig. 3. Surface morphology of Kuraray YP80FP carbon starting material at 1000× magnification (a) and at 2000× magnification (b).

steel current collectors. A high concentration (5 M) was used to maximize ionic strength and minimize the internal resistance of the cell, which is particularly beneficial for electric double-layer capacitor (EDLC) behavior. Moreover, $NaNO_3$ is non-corrosive and less hazardous than acidic or alkaline alternatives, making it well-suited for long-term stability studies and environmentally benign setups [22].

The electrochemical performance of porous carbon materials YP80F and YP80FP have been studied using cyclic voltammetry (CV), galvanostatic charge-discharge (GCPL) and electrochemical impedance spectroscopy. The focus is on the influence of the voltage range on the electrochemical behaviour of the electrode material, and the effect of high temperature treatment on its capacitive properties. The CV method allows to evaluate the electrochemical and kinetic characteristics of reactions in electrical and electrochemical energy storage devices under different conditions [32]. The galvanostatic charge-discharge method was used to analyse specific capacitance and efficiency, which allows the stability of material performance to be assessed at different potentials. The electrochemical impedance spectroscopy method allowed us to determine the changes in internal resistance and charge transfer processes as a function of voltage.

The results obtained allowed us to evaluate how the high temperature treatment of the carbon material affects its porous structure and electrical conductivity, which in turn determines its electrochemical performance. This section presents a detailed analysis and discussion of the effect of various factors on the performance of YP80F and YP80FP carbons in an electrochemical system. The measurements carried out at different upper potentials (0.6 V, 0.8 V, 1.0 V, 1.2 V, 1.4 V, 1.5 V) help to determine the optimum operating voltage range for these materials. The CV were obtained at a scan rate of 2 mV/s in an aqueous solution of 5M $NaNO_3$ as electrolyte. Figure 4 shows the CV for YP80F (a) and YP80FP (b). Comparative tables with capacitance (C, F/g) and efficiency (%) for each voltage range are also shown. As the upper voltage limit increases, the area under the CV curve increases, which indicates an increase in specific capacitance. The graphs have an almost rectangular shape at low voltages (0.6–1.0 V), which is typical of an ideal electrical double layer (EDLC). However, at higher voltages (1.2–1.5 V), a deviation from the rectangular shape is observed, which may indicate the onset of pseudo-capacitive processes. In all voltage ranges, the YP80F shows higher capacitance values than the second sample. For example, at 0.6 V the difference is 81 F/g versus 65 F/g, and at 1.5 V it is 99 F/g versus 85 F/g. This indicates the greater ability of the YP80F to store charge. If we compare the efficiency (Eff., %) of the two carbons, YP80F shows high Coulombic efficiency (more than 99%) at low voltages (0.6–1.0 V), but it decreases to 93% at 1.5 V as the voltage increases. In contrast, YP80FP exhibits lower Coulombic efficiency (99% at 0.6 V), which further decreases to 96% at 1.5 V.

Figure 5 shows comparative CV plots of the carbons at voltage ranges of 0.6 V, 1.0 V and 1.5 V. The plots show typical behaviour of capacitive materials with rectangular shaped curves indicating a pseudo capacitive charge character. YP80F exhibits higher capacitive current compared to YP80FP in all voltage ranges, indicating its higher specific capacitance. As the voltage increases up to 1.5 V, the area bounded by the CV curves becomes larger, indicating an increase in capacitive performance. The CV curves maintain a

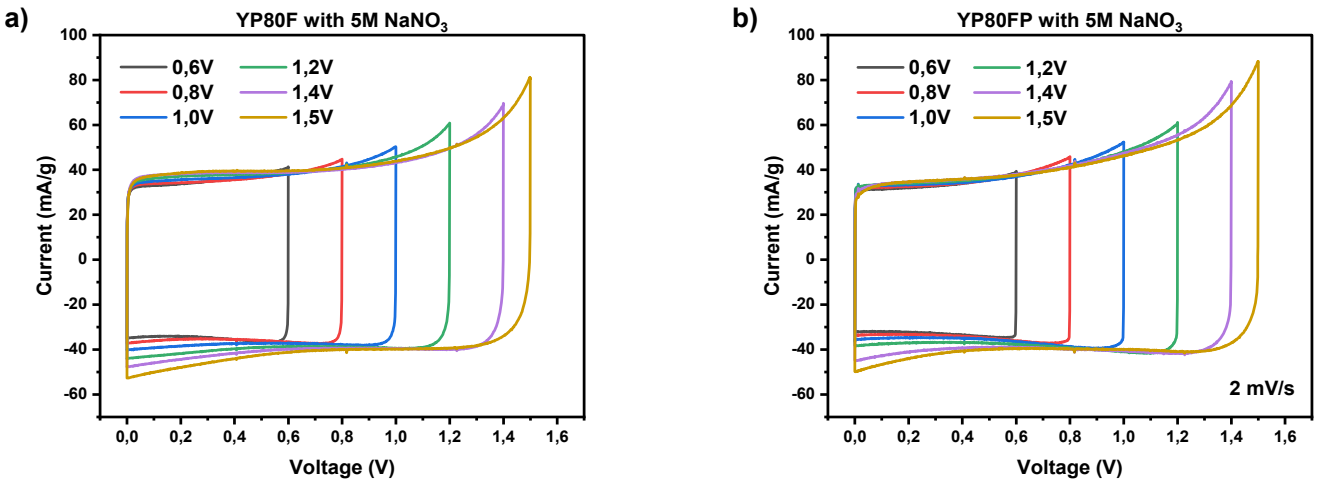

Fig. 4. Cyclic voltammetry for YP80F (a) and YP80FP (b) at scan rate of 2 mV/s at different voltage ranges.

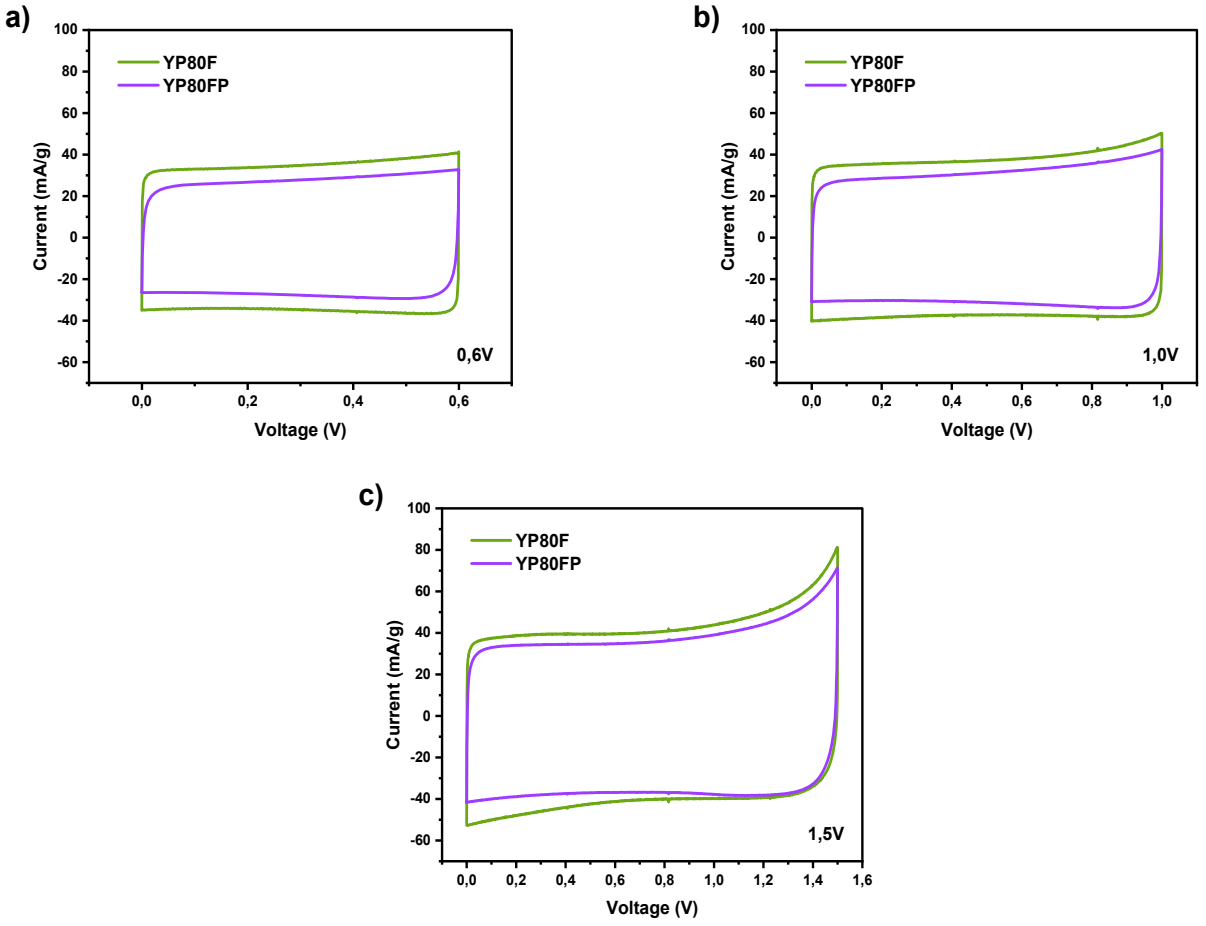

Fig. 5. Comparison of cyclic voltammetry of YP80F (green curve) and YP80FP (violet curve) carbons at voltage ranges of 0.6 V, 1.0 V and 1.5 V.

quasi-rectangular shape, indicating good reversibility and capacitive behavior for both samples. However, YP80F shows more pronounced supercapacitor characteristics, which makes it a more promising material for electrochemical energy storage.

Figure 6a shows the galvanostatic charge-discharge curve for carbon YP80F and Fig. 6b for YP80FP, both were tested in 5M $NaNO_3$ solution at a current density of 200 mA/g. Comparing the data obtained, it can be observed that YP80F shows a higher specific capacitance (up to 106 F/g) compared to YP80FP (up to 92 F/g), which is confirmed by the longer discharge time. The efficiency of both materials remains high (96–100% for YP80F and YP80FP).

According to the results, YP80F shows better performance for supercapacitor applications due to its higher capacitance and longer discharge time.

Figure 7 shows the Coulombic efficiency (CE, %) and specific capacitance (F/g) as a function of potential for YP80F and YP80FP in 5M $NaNO_3$. Both materials show an increase in specific capacitance with increasing potential and a decrease in CE. YP80F has higher specific capacitance (89–106 F/g) compared to YP80FP (75–92 F/g), indicating its better charge storage capacity. However, its CE starts to decrease after 1.2 V, whereas that of YP80FP remains stable (>99%) up to 1.4 V.

Thus, YP80F is suitable for application as an electrode material due to its high specific capacitance, but its stability is limited. In contrast, YP80FP is more stable but inferior in capacitance. The choice between them depends on the priority between charge storage and stability of electrochemical performance.

Figure 8 shows the galvanostatic charge-discharge curves of samples YP80F and YP80FP at different end voltages (0.6 V, 1.0 V, 1.5 V). It can be seen that for all voltages, the discharge times of YP80FP are shorter than that of YP80F, indicating the lower capacitance of YP80FP. The linear and symmetric charge-discharge profiles indicate capacitive behavior typical of electric double-layer capacitors (EDLCs). As the voltage increases, the discharge time increases, which is due to the increase in the available potential for charge accumulation. However, for YP80FP, the shorter discharge time at all potentials may be due to higher resistance or smaller effective charge storage surface.

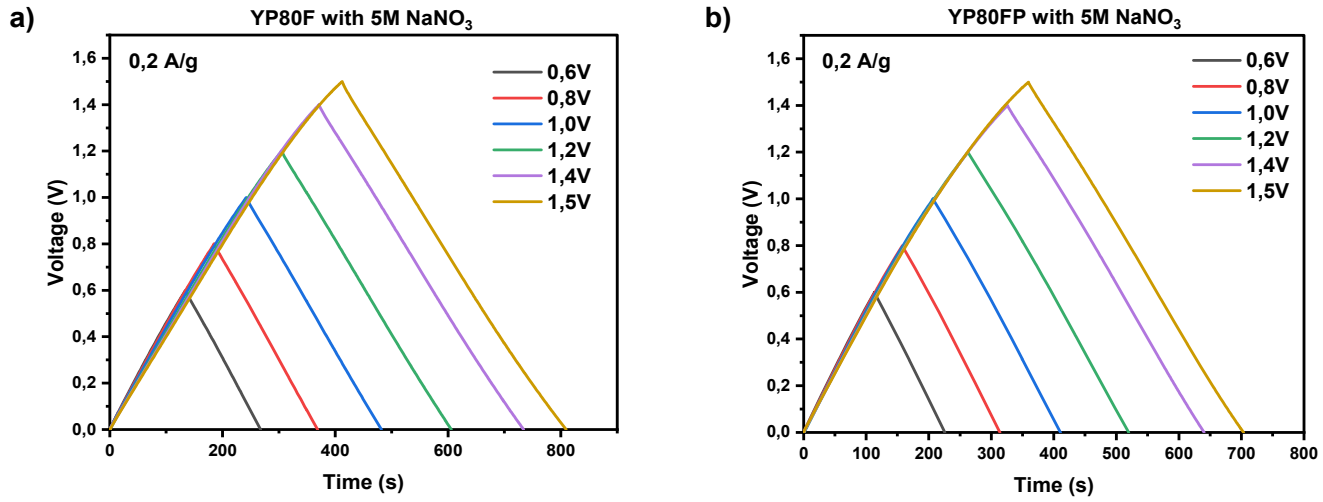

Fig. 6. Galvanostatic charge-discharge curve for YP80F (a) and YP80FP (b) carbons at a current density of 200 mA/g.

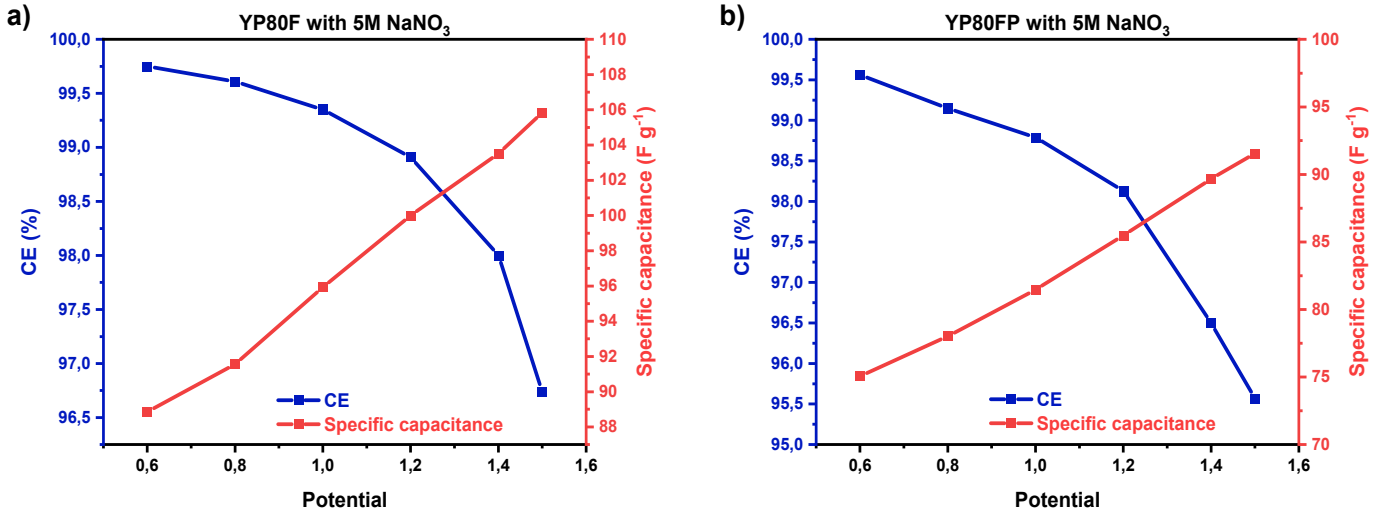

Fig. 7. Voltage dependence of capacitance and energy efficiency up to 1.5 V.

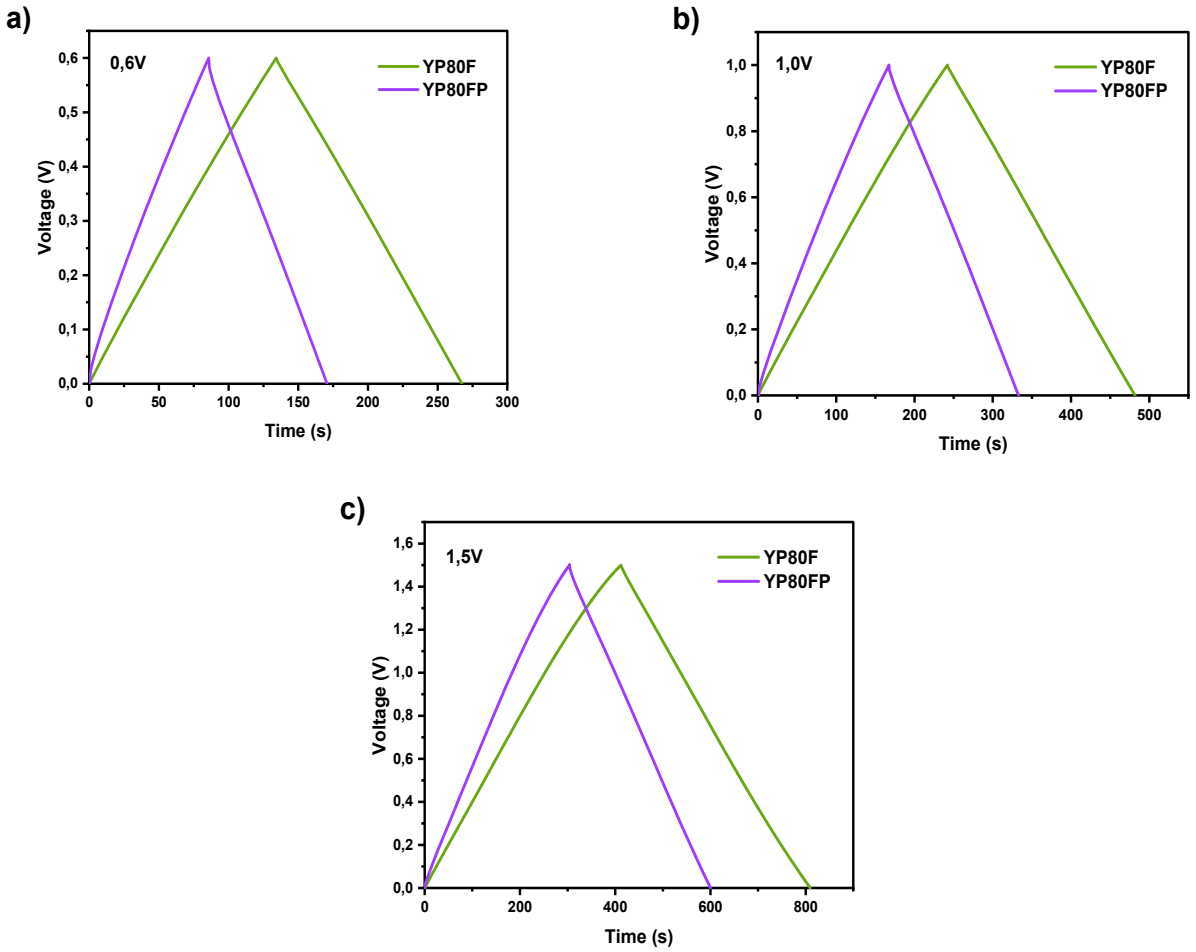

Fig. 8. Comparison of galvanostatic charge-discharge curves of carbon YP80F (green curve) and YP80FP (violet curve) at a current density of 200 mA/g and voltage ranges of 0.6 V, 1.0 V and 1.5 V.

Figure 9 shows the electrochemical impedance (EIS) data for YP80F and YP80FP carbons in 5M $NaNO_3$. Analysis of Nyquist diagrams shows that YP80F has lower impedance compared to YP80FP, indicating better conductivity and more efficient ion diffusion. In the low frequency region, YP80F exhibits lower charge transfer resistance, indicating its high electrode activity. At the same time, a higher total resistance characterizes YP80FP and its curves show indicating increased charge-transfer resistance and pore structure heterogeneity with increasing voltage.

Figure 10 shows the comparison of electrochemical impedance spectra for samples YP80F and YP80FP. In the high frequency region, a small half cycle associated with the charge transfer resistance is observed. In the low frequency region, the low-frequency diffusion slope related to diffusion processes is different for the two samples. YP80FP shows a more pronounced slope, indicating higher diffusion resistance. Sample YP80FP has a higher total resistance (Z'), which also proves the presence of high ohmic and interfacial resistance compared to the results of sample YP80F.

The higher capacitance and lower resistance of YP80F observed in cyclic voltammetry, galvanostatic charge–discharge, and electrochemical impedance analysis can be attributed primarily to its more developed porous structure, which facilitates efficient ion transport and provides a large accessible surface area for charge accumulation. However, porosity is not the only determining factor. Other important contributors include the electrical conductivity of the carbon matrix, the degree of graphitization (which affects charge transfer resistance), the wettability of the surface (which influences electrolyte penetration), and the surface functional groups, which may introduce pseudocapacitive effects or influence interface properties [33, 34]. The results obtained confirm that YP80F demonstrates higher specific capacity, lower charge transfer resistance, and better cycling stability compared to heat-treated YP80FP

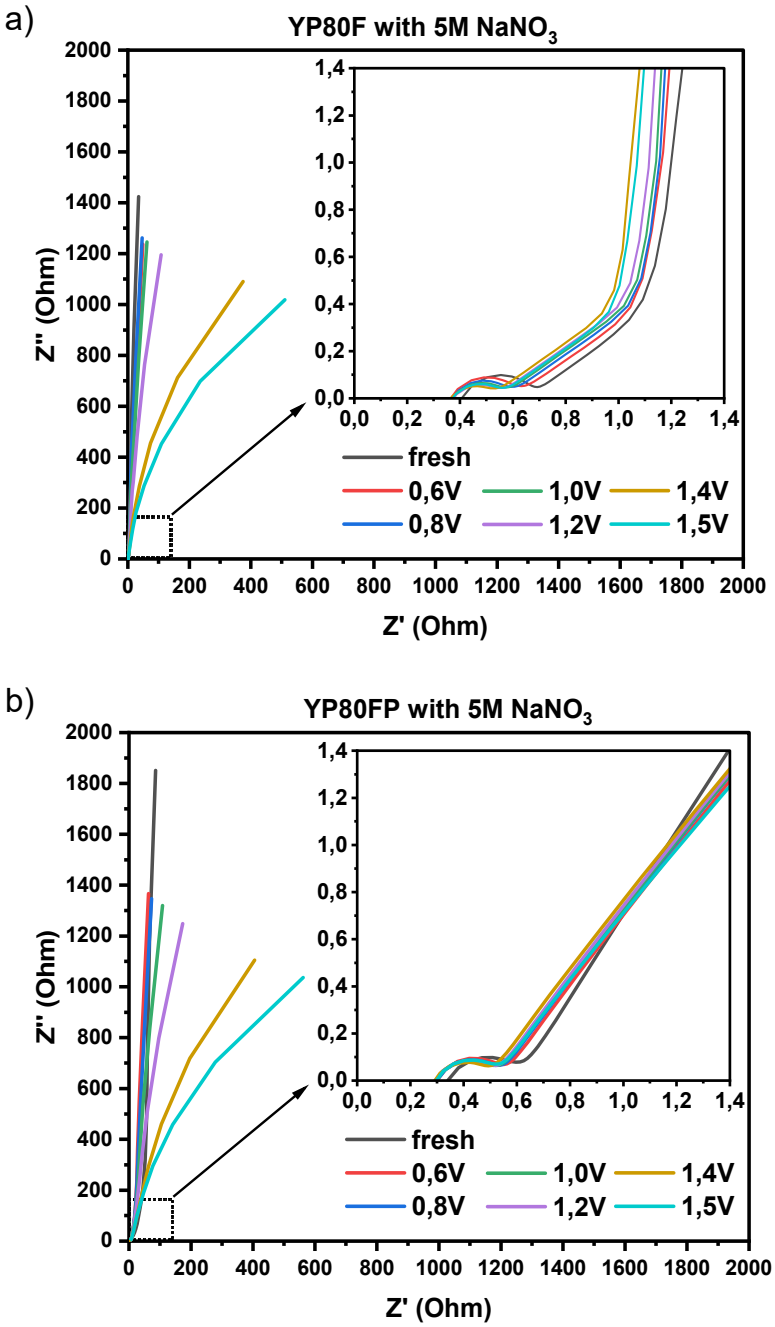

Fig. 9. Electrochemical impedance data for YP80F (a) and YP80FP (b).

(new). However, in addition to the main electrochemical characteristics, an important indicator of the practical suitability of the material is its tendency to self-discharge — an undesirable process of charge loss at rest. This parameter was additionally investigated for both samples and is presented below.

3.4 Self-discharge Behavior of YP80F and YP80FP

Self-discharge is an important performance parameter of supercapacitors, reflecting the ability of the electrode material to retain stored charge over time without external load. In this study, self-discharge behaviour of the YP80F and YP80FP samples was investigated by monitoring the open-circuit potential over a 24-hour period after charging the cells to 1.5 V in 5M $NaNO_3$ electrolyte (Fig. 11). The obtained curves exhibit a characteristic two-stage decay: an initial rapid drop in voltage within the first 2 h, followed by a slower decline in the subsequent 22 hours. This behaviour is typical for electric double-layer capacitors and is attributed to a combination of internal charge redistribution within the porous structure and side reactions involving residual surface functional groups and electrolyte interactions [35].

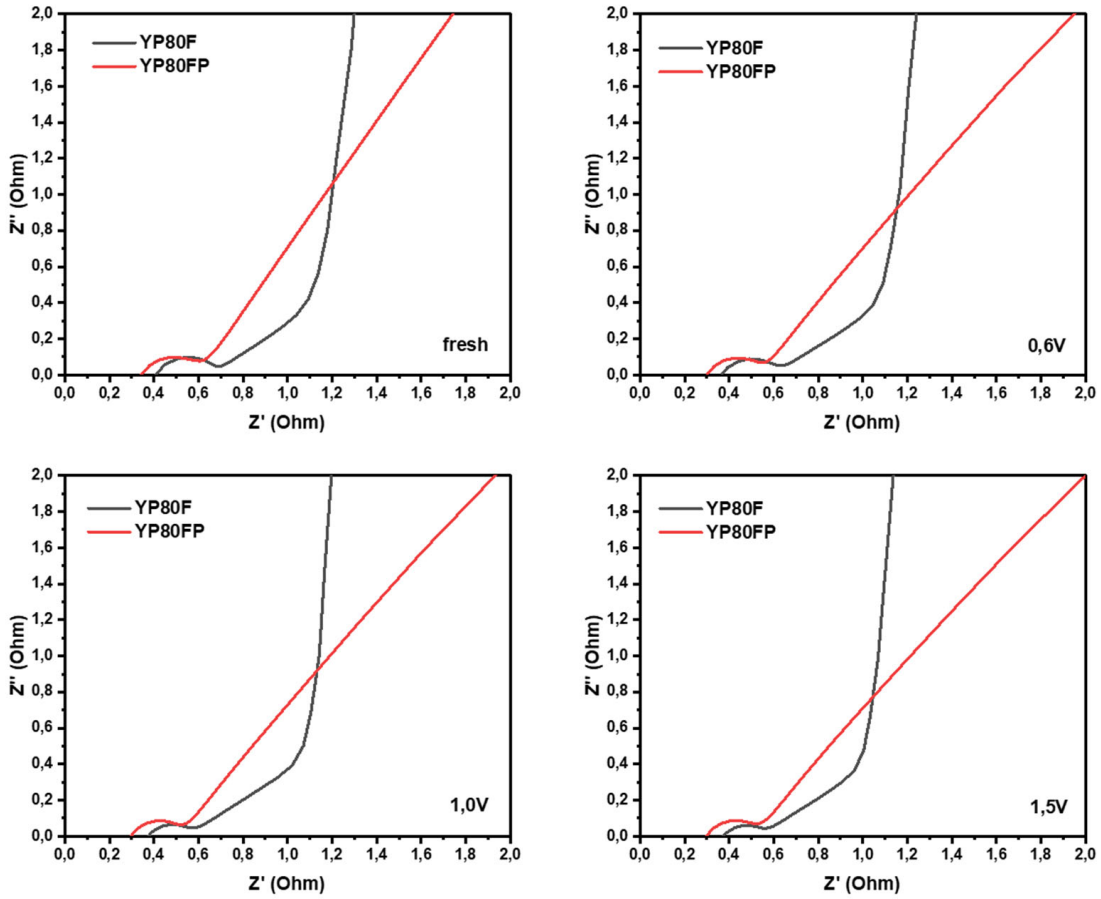

Fig. 10. Comparison of Nyquist plots in high frequency region for supercapacitors with YP80F (black curve) and YP80FP (red curve) carbons.

For YP80F, the voltage dropped from 1.50 V to ~1.22 V in the first 2 h and reached 1.06 V after 24 hours. In contrast, YP80FP showed a faster potential decay, decreasing to ~1.15 V within the same 2-hour interval and reaching 0.95 V at the end of the experiment. The higher self-discharge rate observed for YP80FP may be related to structural compaction and a decrease in surface functional groups as a result of thermal treatment, which could affect ion mobility and reduce the ability to stabilise charge carriers. These results confirm the superior charge retention capability of the untreated YP80F, which correlates with its higher specific capacitance, longer discharge time, and lower internal resistance observed in the galvanostatic tests. Thus, YP80F is more suitable for applications requiring long-term energy retention.

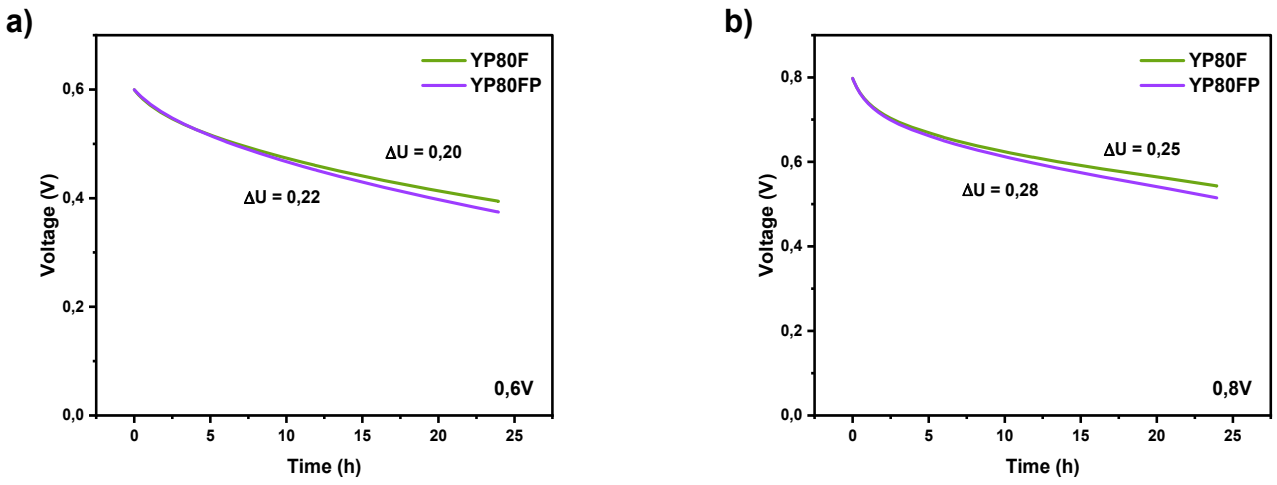

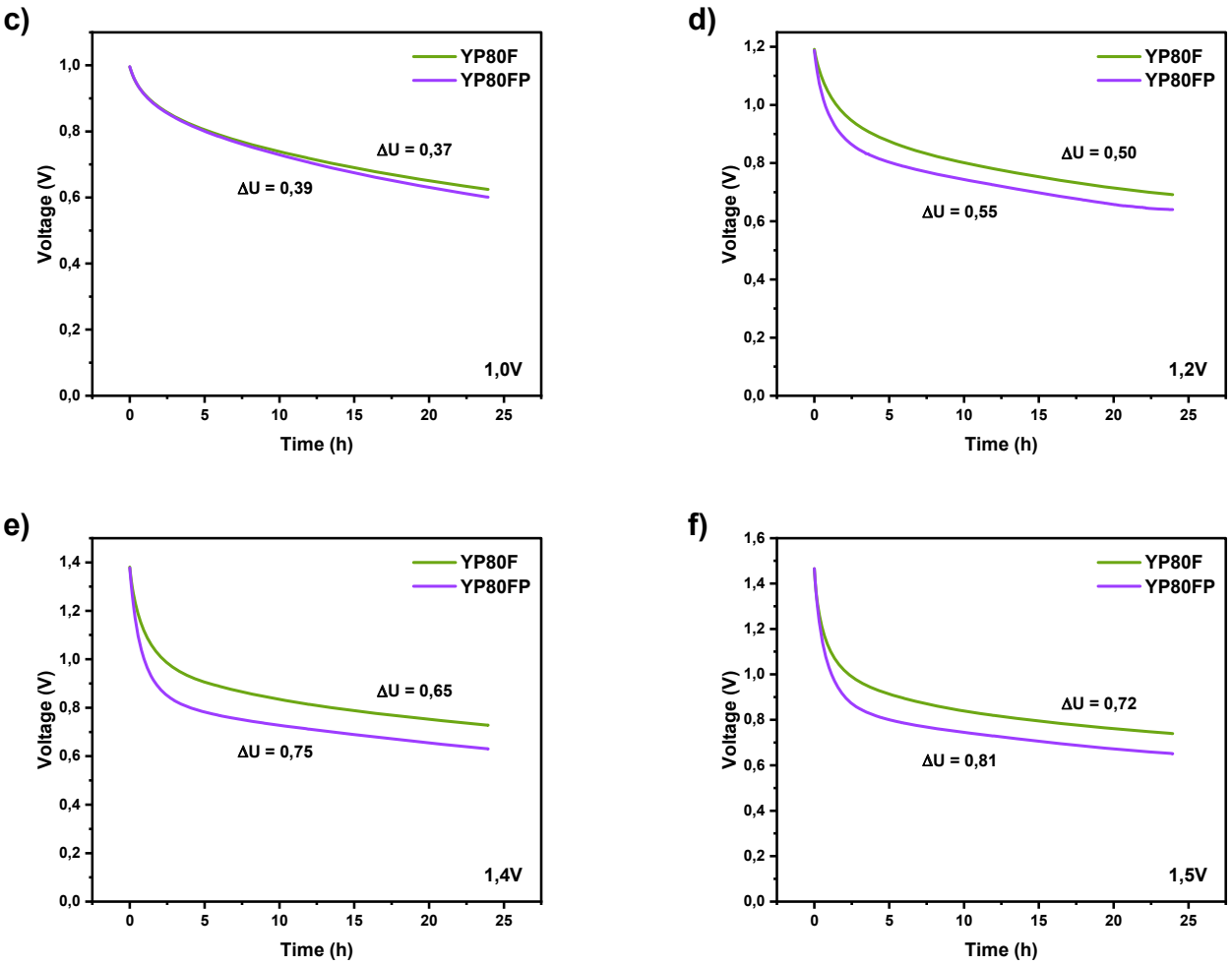

Fig. 11. Self-discharge curves of YP80F and YP80FP at various voltages in 5M $NaNO_3$ over 24 h.

4. Conclusion

In this study, the structural, morphological, and electrochemical properties of commercial activated carbon YP80F and its thermally treated analogue YP-80FP were systematically investigated to assess their suitability for use in aqueous supercapacitors. BET and SEM analyses revealed YP80F possesses a high specific surface area (2346 m^2/g) and predominantly microporous structure (0.9711 cm^3/g, accounting for 79.3% of total pore volume), while YP80FP retained a comparable surface area but exhibited signs of surface densification and pore compaction. Electrochemical tests demonstrated the superior performance of YP80F, with a specific capacitance of 99 F/g at 1.5 V and a maximum value of 106 F/g under galvanostatic charge-discharge conditions. In contrast, YP80FP displayed lower capacitance (maximum 92 F/g) and slightly reduced Coulombic efficiency. YP80F also exhibited longer discharge times, more ideal linear profiles, and lower charge transfer resistance, indicating improved conductivity and ion accessibility. These findings confirm that thermal treatment, although preserving microporosity, can negatively affect electrochemical performance due to changes in surface morphology and conductivity pathways. Therefore, optimizing treatment conditions is essential to maintain the balance between structural stability and electrochemical efficiency in activated carbon electrodes for supercapacitor applications.

Acknowledgments

This research has been funded by the Committee of Science of the Ministry of Science and Higher Education of the Republic of Kazakhstan (Grant No. BR27198045).

References

[1]. A. Li, S. Kong, C. Guo, H. Ooka, et al., Enhancing the stability of cobalt spinel oxide towards sustainable oxygen evolution in acid, *Nat. Catal.* 5 (2022) 109-118. DOI: 10.1038/s41929-021-00732-9

[2]. C. Cometto, A. Ugolotti, E. Grazietti, A. Moretto, et al., Copper single-atoms embedded in 2D graphitic carbon nitride for the CO_2 reduction, *npj 2D Mater. Appl.* 5 (2021) 63. DOI: 10.1038/s41699-021-00243-y

[3]. O. Alduhaish, M. Ubaidullah, A.M. Al-Enizi, N. Alhokbany, et al., Facile synthesis of mesoporous α-Fe_2O_3@g-C_3N_4-NCs for efficient bifunctional electro-catalytic activity (OER/ORR), *Sci. Rep*. 9 (2019) 14139. DOI: 10.1038/s41598-019-50780-2

[4]. D.K. Sam, S. Gong, A. Durairaj, E.K. Sam, et al., Fabrication of highly dispersed Mo_2C coupled with Co-N-C via self-template as bifunctional electrocatalysts, *Int. J. Energy Res*. 45 (2021) 10989–11001. DOI: 10.1002/er.6583

[5]. M. Reina, A. Scalia, G. Auxilia, M. Fontana, et al., Boosting electric double layer capacitance in laser-induced graphene-based supercapacitors, *Adv. Sustain. Syst.* 6 (2022) 2100228. DOI: 10.1002/adsu.202100228

[6]. Y. Feng, H. Zhang, W. Li, L. Fang, Y. Wang. Targeted synthesis of novel hierarchical sandwiched NiO/C arrays as high-efficiency lithium ion batteries anode, *J. Power Sources* 301 (2016) 78–86. DOI: 10.1016/j.jpowsour.2015.09.101

[7]. H.L. Ferreira, R. Garde, G. Fulli, W. Kling, J.P. Lopes. Characterisation of electrical energy storage technologies, *Energy* 53 (2013) 288–298. DOI: 10.1016/j.energy.2013.02.037

[8]. X. Zhang, Z. Li, L. Luo, Y. Fan, Z. Du. A review on thermal management of lithium-ion batteries for electric vehicles, *Energy* 238 (2022) 121652. DOI: 10.1016/j.energy.2021.121652

[9]. Q. Abbas, M. Mirzaeian, M.A. Abdelkareem, A. Al Makky, et al., Structural tuneability and electrochemical energy storage applications of resorcinol-formaldehyde-based carbon aerogels, *Int. J. Energy Res*. 46 (2022) 5478–5502. DOI: 10.1002/er.7556

[10]. W. Münchgesang, P. Meisner, G. Yushin. Supercapacitors specialities – Technology review, *AIP Conf. Proc.* 1597 (2014) 196–203. DOI: 10.1063/1.4878488

[11]. G. Ren, G. Ma, N. Cong. Review of electrical energy storage system for vehicular applications, *Renew. Sustain. Energy Rev.* 41 (2015) 225–236. DOI: 10.1016/j.rser.2014.08.003

[12]. S. Parveen, S.K. Sharma, S.N. Pandey. High performance solid state symmetric supercapacitor based on reindeer moss-like structured $Al(OH)_3$/MnO_2/FeOOH composite electrode for energy storage applications, *Energy* 224 (2021) 120137. DOI: 10.1016/j.energy.2021.120137

[13]. J.R. Miller, A. Burke. Electrochemical capacitors: challenges and opportunities for real-world applications, *Electrochem. Soc. Interface* 17 (2008) 53. DOI: 10.1149/2.F08081IF

[14]. S. Faraji, F.N. Ani. The development supercapacitor from activated carbon by electroless plating – A review, *Renew. Sustain. Energy Rev*. 42 (2015) 823-834. DOI: 10.1016/j.rser.2014.10.068

[15]. H. Chen, T.N. Cong, W. Yang, C. Tan, et al., Progress in electrical energy storage system: A critical review, *Prog. Nat. Sci.* 19 (2009) 291–312. DOI: 10.1016/j.pnsc.2008.07.014

[16]. M. Mirzaeian, Q. Abbas, A. Ogwu, P. Hall, et al., Electrode and electrolyte materials for electrochemical capacitors, *Int. J. Hydrogen Energy* 42 (2017) 25565-25587. DOI: 10.1016/j.ijhydene.2017.04.241

[17]. L. Sun, Y. Gong, D. Li, C. Pan. Biomass-derived porous carbon materials: synthesis, designing, and applications for supercapacitors, *Green Chem*. 24 (2022) 3864–3894. DOI: 10.1039/D2GC00099G

[18]. F. Díaz-González, A. Sumper, O. Gomis-Bellmunt, R. Villafáfila-Robles. A review of energy storage technologies for wind power applications, *Renew. Sustain. Energy Rev*. 16 (2012) 2154-2171. DOI: 10.1016/j.rser.2012.01.029

[19]. D.K. Sam, H. Li, Y.T. Xu, Y. Cao. Porous carbon fabrication techniques: a review, *J. Ind. Eng. Chem*. 135 (2024) 17-42. DOI:10.1016/j.jiec.2024.01.044

[20]. M. Thommes, K.A. Cychosz, A.V. Neimark. Advanced physical adsorption characterization of nanoporous carbons. In: Novel Carbon Adsorbents (2012) 107–145. DOI: 10.1016/B978-0-08-097744-7.00004-1

[21]. X. Li, Y. Zhao, Y. Yang, S. Gao. A universal strategy for carbon-based ORR-active electrocatalyst: one porogen, two pore-creating mechanisms, three pore types, *Nano Energy* 62 (2019) 628–637. DOI: 10.1016/j.nanoen.2019.05.066

[22]. Zh. Supiyeva, X. Pan, Q. Abbas. The critical role of nanostructured carbon pores in supercapacitors, *Curr. Opin. Electrochem*. 39 (2023) 101249. DOI: 10.1016/j.coelec.2023.101249

[23]. M. Hartmann, W. Schwieger. Hierarchically-structured porous materials: from basic understanding to applications, *Chem. Soc. Rev.* 45 (2016) 3311–3312. DOI: 10.1039/C6CS90043G

[24]. X.Y. Yang, L.H. Chen, Y. Li, J.C. Rooke, et al., Hierarchically porous materials: synthesis strategies and structure design, *Chem. Soc. Rev.* 46 (2017) 481–558. DOI: 10.1039/c6cs00829a

[25]. V. Thangadurai, S. Narayanan, D. Pinzaru. Garnet-type solid-state fast Li ion conductors for Li

batteries: critical review, *Chem. Soc. Rev.* 43 (2014) 4714-4727. DOI: 10.1039/c4cs00020

[26]. V. Aravindan, W. Chuiling, M.V. Reddy, G.S. Rao, et al., Carbon coated nano-$LiTi_2(PO_4)_3$ electrodes for non-aqueous hybrid supercapacitors, *Phys. Chem. Chem. Phys.* 14 (2012) 5808-5814. DOI: 10.1039/c2cp40603a

[27]. T. Placke, R. Kloepsch, S. Dühnen, M. Winter. Lithium ion, lithium metal, and alternative rechargeable battery technologies: the odyssey for high energy density, *J. Solid State Electrochem.* 21 (2017) 1939-1964. DOI: 10.1007/s10008-017-3610-7

[28]. H. Kim, J. Hong, K.Y. Park, H. Kim, et al., Aqueous rechargeable Li and Na ion batteries, *Chem. Rev*. 114 (2014) 11788-11827. DOI: 10.1021/cr500232y

[29]. N. Jabeen, A. Hussain, Q. Xia, S. Sun, et al., High-Performance 2.6 V Aqueous Asymmetric Supercapacitors based on In Situ Formed $Na_{0.5}MnO_2$ Nanosheet Assembled Nanowall Arrays, *Adv. Mater.* 29 (2017) 1700804. DOI: 10.1002/adma.201700804

[30]. J. Iqbal, A. Numan, S. Rafique, R. Jafer, et al., High performance supercapattery incorporating ternary nanocomposite of multiwalled carbon nanotubes decorated with Co_3O_4 nanograins and silver nanoparticles as electrode material, *Electrochim. Acta* 278 (2018) 72-82. DOI: 10.1016/j.electacta.2018.05.040

[31]. M. Sajjad, M.I. Khan, F. Cheng, W. Lu. A review on selection criteria of aqueous electrolytes performance evaluation for advanced asymmetric supercapacitors, *J. Energy Storage* 40 (2021) 102729. DOI: 10.1016/j.est.2021.102729

[32]. A.S. Aderyani, P. Flouda, S. Shah. Simulation of cyclic voltammogram in structural supercapacitors with pseudocapacitance behavior, *Electrochim. Acta* 390 (2021) 138822. DOI: 10.1016/j.electacta.2021.138822

[33]. W. Pholauyphon, P. Charoen-amornkitt, T. Suzuki, S. Tsushima. Guidelines for supercapacitor electrochemical analysis: A comprehensive review of methodologies for finding charge storage mechanisms, *J. Energy Storage* 98 (2024) 112833. DOI: 10.1016/j.est.2024.112833

[34]. K. Xue, L. Fang, G. Zhang, M. Yu, et al., The evaluation of microstructure of carbon/carbon composites generated by ultra-high temperature treatment towards excellent electromagnetic interference shielding property, *Carbon* 193 (2022) 128-139. DOI: 10.1016/j.carbon.2022.03.031

[35]. Abbas Q., Béguin F. Influence of the iodide/iodine redox system on the self-discharge of AC/AC electrochemical capacitors in salt aqueous electrolyte, *Prog. Nat. Sci.: Mater. Int*. 25 (2015) 622-630. DOI: 10.1016/j.pnsc.2015.12.002